

Sensitivity of CMS to the LFV Neutrinoless $\tau \rightarrow 3\mu$ decay using W Sources

Experimental Project Report

Supervisor: James D. Olsen

Siddharth Mishra Sharma¹

Princeton University

(Dated: 25 October 2014)

In this note we present a study of the sensitivity of the CMS detector to the lepton flavor violating (LFV) decay $\tau \rightarrow 3\mu$ obtainable using 19.5 fb^{-1} of 2012 proton-proton collision data at $\sqrt{s} = 8 \text{ TeV}$ and W bosons as sources of τ . The expected upper limit on the branching fraction in this case is found to be $\mathcal{B}(\tau \rightarrow 3\mu) < 2.3 \times 10^{-7}$ at 95% CL. This result is about an order of magnitude worse than current experimental limits set at the B -factories Belle and BaBar.

I. INTRODUCTION

A. Theoretical motivation

Although lepton flavor is conserved within the Standard Model (SM) of particle physics, inclusion of massive neutrinos (which follows from the experimental observation of neutrino oscillations) allows for the possibility of lepton flavor violating (LFV) processes. The branching fraction for such processes would be negligible due to small neutrino mass and cancellations from the GIM mechanism¹. However, many Beyond Standard Model (BSM) theories including certain permutations of supersymmetry and large extra dimensions predict an enhancement in the branching fraction of LFV decays to ranges potentially observable using current experiments². As such, any observation of such processes would be an unambiguous sign of new physics. The high LHC luminosity puts CMS in a good position to search for low branching fraction decays of this sort, such as the very rare $B_s^0 \rightarrow \mu\mu$ process recently first observed at CMS and LHCb^{3,4}.

B. Current experimental limits

The current best experimental upper limits on this decay are $\mathcal{B}(\tau^- \rightarrow \mu^-\mu^+\mu^-) < 2.1 \times 10^{-8}$ at 90% confidence level (CL) from Belle⁵ and $\mathcal{B}(\tau^- \rightarrow \mu^-\mu^+\mu^-) < 3.3 \times 10^{-8}$ at 90% CL from BaBar⁶. A recent measurement by LHCb produced an upper limit of $\mathcal{B}(\tau^- \rightarrow \mu^-\mu^+\mu^-) < 4.6 \times 10^{-8}$ at 90% CL⁷. Copious τ production and a relatively clean signal makes B -factories well suited to study this type of process.

C. τ sources

The main sources of τ leptons at the LHC are decays of W bosons, Z bosons, D mesons and B mesons. The order-of-magnitude production cross sections for these processes are^{8,9}

- $\sigma(pp \rightarrow W \rightarrow \tau\nu_\tau) = \mathcal{O}(10 \text{ nb})$

- $\sigma(pp \rightarrow Z \rightarrow \tau\tau) = \mathcal{O}(1 \text{ nb})$
- $\sigma(pp \rightarrow B \rightarrow \tau + X) = \mathcal{O}(10 \mu\text{b})$
- $\sigma(pp \rightarrow D_s \rightarrow \tau\nu_\tau) = \mathcal{O}(10 \mu\text{b})$

While substantially more τ leptons are produced from the mesons, these are relatively soft (lower p_T) which makes the daughter muons substantially harder to trigger on and properly reconstruct. Although τ s from the meson decays are potentially viable sources in searching for LFV decays, in this note we study τ s from W sources, which are characterized by higher p_T and an accompanying neutrino which manifests itself as missing transverse energy (MET).

II. THE EXPERIMENT

A. Large Hadron Collider

The Large Hadron Collider¹⁰ (LHC) is a circular proton-proton collider 27 km in circumference located near Geneva, Switzerland straddling the French-Swiss border. Four principal experiments are located at the LHC: CMS, ATLAS, LHCb and ALICE. ATLAS and CMS are general-purpose detectors aimed at exploring a wide range of Standard Model and Beyond Standard Model phenomena, while ALICE and LHCb are more specialized experiments dedicated to studying physics of strongly interacting matter (quark-gluon plasma) at high energy densities and flavor physics related to CP violation respectively.

The first successful pp collisions at the LHC were recorded in 2009, with roughly 5 fb^{-1} of data at center-of-mass energy $\sqrt{s} = 7 \text{ TeV}$ and 20 fb^{-1} of data at $\sqrt{s} = 8 \text{ TeV}$ taken during the 2011 and 2012 data-taking periods respectively. The LHC will resume operations in 2015 closer to its design energy of $\sqrt{s} = 14 \text{ TeV}$.

B. Compact Muon Solenoid

The Compact Muon Solenoid^{11,12} (CMS) is a general-purpose detector at the LHC designed to search for and

constrain the properties of SM particles as well as to look for signs of new physics such as supersymmetry, extra dimensions and dark matter. Here we only provide a brief overview of the sub-components of the detector and aspects of its functioning relevant to our study. A schematic view of CMS showing its sub-components is shown in Figure 1.

The CMS coordinate system is defined such that the z -axis points in the clockwise beam direction when looking from above, the y -axis is perpendicular to the earth and the x -axis points radially inwards. Azimuthal angle ϕ is measured in the x - y plane from the x -axis and polar angle θ from the z -axis. Polar coordinates are usually quoted in terms of pseudorapidity $\eta \equiv -\ln(\tan \frac{\theta}{2})$. Distances in η - ϕ space are then given by $\Delta R = \sqrt{\Delta\eta^2 + \Delta\phi^2}$.

1. Tracking system

The CMS tracking system is the innermost component of the detector and consists of silicon pixel and strip detectors immersed in a 3.8T coaxial magnetic field from the CMS solenoid. Its purpose is to reconstruct tracks representing the trajectories of incident charged particles by registering hits on the approximately 76 million individual pixel and strip components.

Track reconstruction involves using pattern recognition and fitting in several iterations to estimate the optimal trajectory parameters of the charged particles. Trajectory curvature due to the magnetic field allows for measurements of the transverse momentum (p_T) with a resolution of $\sim 1.5\%$ for particles in the most relevant kinematic range.

2. Electromagnetic calorimeter

The electromagnetic calorimeter (ECAL) is the next sub-component and is located just outside the silicon tracker. Made of lead tungstate crystals, its main purpose is to measure the energy of electrons and photons to a good resolution (1-2%).

3. Hadronic calorimeter

The hadronic calorimeter (HCAL) is made of alternating layers of brass plates and plastic scintillator. Its purpose is to measure the energy of hadrons, which allows for the reconstruction of hadronic jets and, together with the ECAL, measurements of the missing transverse energy (MET).

4. Muon system

The CMS muon system¹³ is the outermost sub-component in the detector and is used to identify and reconstruct the trajectories of muons. Being minimum ionizing particles, muons generally do not interact with the inner components of the detector and can be detected in the low-radiation environment of the muon system. Since in this study we are primarily dealing with all-muon final states, it is worth briefly mentioning some details of muon identification and reconstruction.

Due to varying conditions in different coverage regions of the detector, three different detector technologies are employed in the muon system¹³. Drift tube chambers (DTs) are used in the barrel ($|\eta| < 1.2$) where the residual magnetic field and muon rates are relatively low. Cathode strip chambers (CSCs) are used in the endcap regions ($0.9 < |\eta| < 2.4$) where these rates are high. Additionally, resistive plate chambers (RPCs) having faster response but coarser position resolution are used in both regions.

During muon reconstruction, information from the muon system is combined with output from other sub-components in different ways to produce the following muon collections¹⁴:

- **Standalone muons:** These are track fits produced by collating information from all components of the muon system alone.
- **Tracker muons:** Hits in the muon system are tested for compatibility with tracks produced from inner tracker information and used to identify and fit potential muon tracks.
- **Global muons:** Standalone muon tracks are matched to those in the inner tracker, and a fit using all hits from both components is performed. Global muons are widely used in physics analyses.
- **Particle Flow muons:** The CMS Particle Flow¹⁵ (PF) algorithm is used to reconstruct particles (including muons) in the event by making use of all sub-component information in order to distinguish different stable particle hypotheses. The reconstructed particles produced from the PF output can then be used in higher level algorithm to produce e.g. isolation and MET information.

Additionally, baseline muon selection criteria as recommended by the muon POG (Physics Object Group) are often used for selecting a subset of reconstructed muons suited for a given analysis¹⁴. For example, for a muon to pass “tight” quality requirements, in addition to being reconstructed as a global and PF muon it must satisfy additional requirements on number of hits and normalized χ^2 of the global muon fit, among others.

5. Trigger

While running, the rate of collision at CMS as delivered by the LHC is about 15 MHz. Due to storage limitations and the high instantaneous luminosity at the LHC a trigger system is required that only keeps events of potential physics interest. The CMS trigger system is designed for this purpose and is able to reduce the event rate to about 500 MHz¹⁶.

The trigger system is two-tiered – the Level 1 (L1) trigger is a set of electronics that performs coarse object reconstruction and uses this information to flag events for acceptance. The maximum allowed output rate at this stage is 100 kHz. The next stage is the High Level Trigger (HLT) that uses software reconstruction of objects closely following offline reconstruction to make acceptance decisions. There are about 500 HLT trigger paths available, and these are selected based on the specific requirements of the analysis.

III. DATA AND SIMULATION

A. Signal Monte Carlo samples

Signal Monte Carlo samples were generated using the PYTHIA event generator by forcing a τ from $W \rightarrow \tau\nu_\tau$ to decay to 3 muons. 20,000 events were produced with pure phase space and flat angular distribution. The difference observed in the p_T distribution of muons obtained by including model specific matrix elements is known to be negligible⁹. The p_T and η distribution of the muons at generator level as well as the minimum and maximum distance between any pair of muons is shown in Figure 2

B. Background Monte Carlo samples

The Monte Carlo samples used in this study were:

- W+jets MC: /WJetsToLNu_8TeV-madgraph-tarball/Summer12_DR53X-PU_S10_START53_V7A-v1/AODSIM (10^7 events)
- Z+jets MC: /DYToMuMu_M-20_CT10_TuneZ2star_v2_8TeV-powheg-pythia6/Summer12_DR53X-PU_RD1_START53_V7N-v1/AODSIM (10^7 events)
- QCD MC: /QCD_Pt_20_MuEnrichedPt_15_TuneZ2star_8TeV_pythia6/Summer12_DR53X-PU_S10_START53_V7A-v3/AODSIM ($\sim 2 \times 10^7$ events)

C. Triggers

The lowest unprescaled single, double and triple muon triggers as well as a dedicated $\tau \rightarrow 3\mu$ trigger were considered for the study. These are respectively

- HLT_IsoMu24: Single isolated muon with $p_T > 24$ GeV.
- HLT_Mu17_Mu8: $p_T^1 > 17$ GeV, $p_T^2 > 8$ GeV.
- HLT_TripleMu5: $p_T^{1,2,3} > 5$ GeV.
- HLT_Tau2Mu_ItTrack: See below.

The signal trigger and preselection efficiencies obtained are shown in Table I. We see that using the dedicated trigger results in a considerably better signal efficiency compared to the others, and this was used throughout the rest of the study. The selection criteria for this trigger are:

- Dimuon invariant mass $M(\mu\mu) > .6$ GeV
- Trimuon invariant mass $M(\mu\mu\mu) > 1.7$ GeV
- Flight length in transverse plane (significance) $L_{xy}^{\text{sig}} > 1$
- Pointing angle $\cos \alpha_{\text{PA}} > .98$
- Trimuon secondary vertex $\chi^2/\text{ndof} < 2$
- Dimuon secondary vertex χ^2 probability $> .1$ (any two muons in the event)

The pointing angle α_{PA} is defined as the angle between the reconstructed τ momentum (equal to the sum of daughter momenta) and the vector pointing from the primary vertex (PV) to the secondary vertex (SV). The W has an extremely short lifetime and decays very close to the PV, and since there are no other neutrinos involved α_{PA} should be very close to zero for a well-reconstructed candidate.

Trigger	$\epsilon_{\text{trigger}} (\%)$	$\epsilon_{\text{presel}} (\%)$
HLT_Mu17_Mu8	13.2	7.4
HLT_IsoMu24	11.3	3.9
HLT_TripleMu5	6.2	5.4
HLT_Tau2Mu_ItTrack	18.5	12.3

TABLE I: Signal trigger and preselection efficiencies for different triggers.

D. Data samples

The data sample used for the main part of the study is /MuOnia/Run2012B-13Jul2012-v1/AOD corresponding to $\int \mathcal{L} dt = 4421 \text{ pb}^{-1}$ which is just under a quarter of the data collected by CMS during the 2012 run. This dataset contains events from the dedicated $\tau \rightarrow 3\mu$ trigger path. Luminosity mask Cert_190456-208686_8TeV_PromptReco_Collisions12_JSON contains a list of “good” runs and was used to filter which luminosity blocks should be processed.

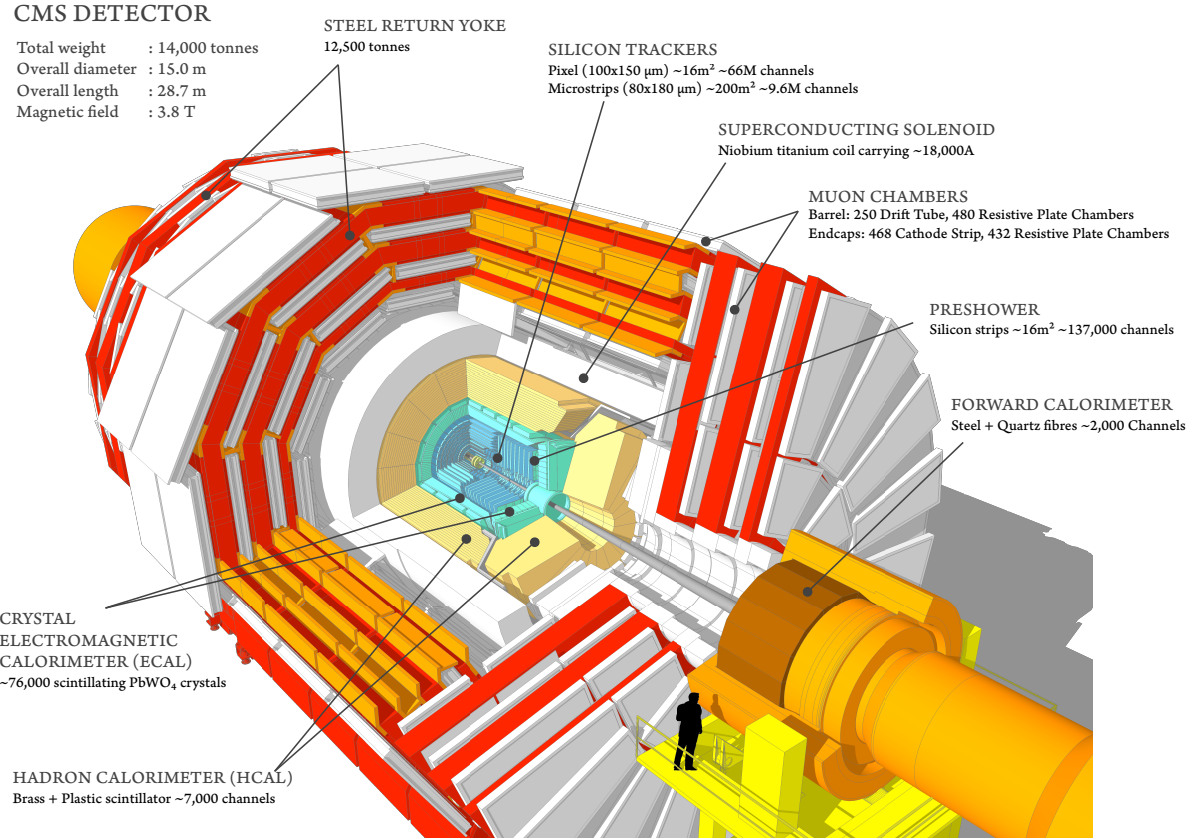


FIG. 1: Layout of the CMS detector showing its sub-components.

IV. ASIDE: ONE AND TWO MUON SELECTION

As a systematic check leading up to the 3 muon case, we reconstructed single and double muon final states from a small sample of data (/SingleMu/Run2012C-PromptReco-v1/AOD corresponding to $\int \mathcal{L} dt = 495 \text{ pb}^{-1}$) using a loose preselection and compared this to $W+jets$, $Z+jets$ and QCD Monte Carlo samples. HLT_IsoMu24 trigger was used with cuts $p_T^1 > 25 \text{ GeV}$, $|\eta| < 2.1$ and muon selection corresponding to “tight” muon ID.

As expected, the single muon case is dominated by $W \rightarrow \mu\nu$ events and the double muon case by $Z \rightarrow \mu\mu$ events. MC samples are individually normalized to the data luminosity. Good agreement between data and MC also serves to validate the MC samples we use in this study. Some variables after selection requiring two muons is shown in Figure 3.

In each case, QCD dominates the lower p_T end of the spectrum for both muons, where a prominent QCD peak is observed. Since the muons are primary daughters of the W/Z in this case, we would expect a significant portion of the inclusive W and Z background events to be excluded by a mass cut around the τ mass.

V. EVENT PRESELECTION

Candidate $\tau \rightarrow 3\mu$ events are preselected by requiring three tracks having an invariant mass close to the τ mass and forming a displaced vertex. As can be seen from Figure 2(e), muons from W decays are highly collimated. This leads to several issues while reconstructing the three-pronged decay, such as muons being matched to the wrong track. In this case reconstruction of one or more muons fails. To partially mitigate this, we consider final states with two muons and a nearby track in addition to those with three reconstructed muons. This is done as follows.

We initially ask for two muons and a nearby track. The muons are required to satisfy quality criteria corresponding to “tight” muon ID, and the track is required to have > 6 valid hits in the tracker with a normalized track-fit $\chi^2 < 5$. If the track is associated to a suitable muon satisfying our quality criteria, we work with the three muons. If not, two muons and the nearby track are used. A three-track vertex fit is then performed using a Kalman Vertex Fitter¹⁷, and the two highest- p_T tracks are vertexed separately. Including a nearby track in the reconstruction improves the signal efficiency by about a factor of 2.

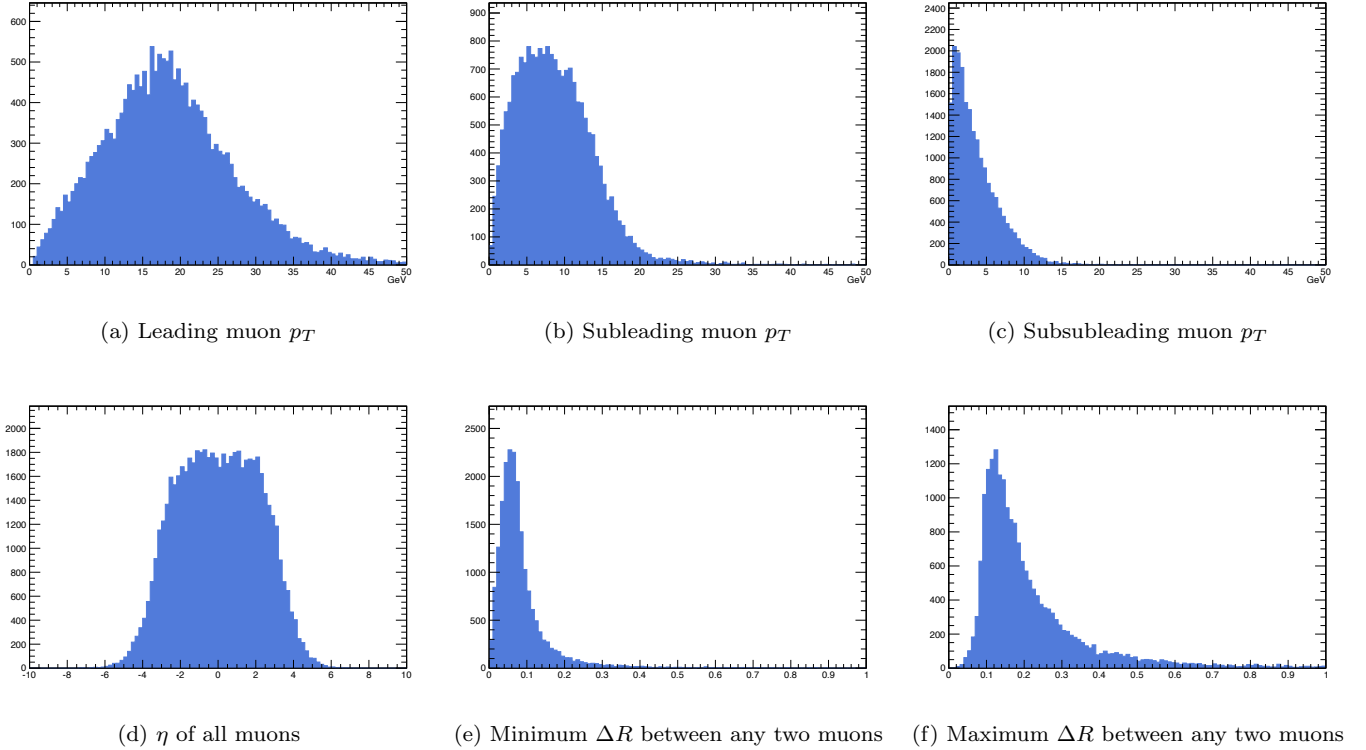


FIG. 2: Some kinematic variables for the signal Monte Carlo at generator level.

The following fairly loose preselection criteria are then applied to the reconstructed events.

- Kinematic cuts: $p_T^{1,2,3} > 3 \text{ GeV}$, $|\eta| < 2.4$
- Vertex cut: dimuon (two leading) SV χ^2 probability $> .02$
- Mass cut: reconstructed candidate mass within $m_\tau(1.7768 \text{ MeV}) \pm 0.0700 \text{ MeV}$
- Pointing angle cut: $\cos \alpha_{PA} > .98$

VI. SIGNAL AND BACKGROUND DISCRIMINATION

The signal region is defined by the mass window $M(\mu\mu\mu) \in [1.75, 1.80]$ corresponding to about 3σ (Figure 4) and we look at data in the mass sidebands. Good agreement between data and the QCD Monte Carlo shows that our background is dominated by QCD events with negligible contribution from $W/Z+jets$, and that the MC does a good job of modeling this background.

Daughter tracks from preselected candidates in the QCD MC can be truth-matched to generator level objects in order to elucidate the source of background processes and come up with suitable selection criteria. We see that the dominant physical background after preselection involves cascades of B and D mesons decaying to

muons, for example

$$D_s^+ \rightarrow \phi \mu^+ \nu_\mu \\ \hookrightarrow \mu^+ \mu^-.$$

Good discriminating variables are identified and cuts found by using a coarse scan to optimize for the Punzi figure of merit, defined by¹⁸

$$\text{FOM}_{\text{Punzi}} \equiv \frac{\epsilon_{\text{sig}}}{N_\sigma/2 + \sqrt{N_{\text{bkg}}}},$$

where ϵ_{sig} is the signal efficiency, N_{bkg} the background yields and N_σ is the required number of standard deviations in the result, which we set to 2 to correspond to a 95% confidence limit. Obtained values are then manually adjusted by optimizing for the expected upper limit on the branching fraction.

Because the background 3μ mass distribution is expected to be uniform, we calculate the expected number of background events for 19.5 fb^{-1} by linearly extrapolating the number of events into the signal region.

A. Kinematic cuts

$\tau \rightarrow 3\mu$ events from Ws are characterized by three highly collimated muons from a boosted τ with p_T somewhat higher than those from QCD background. There

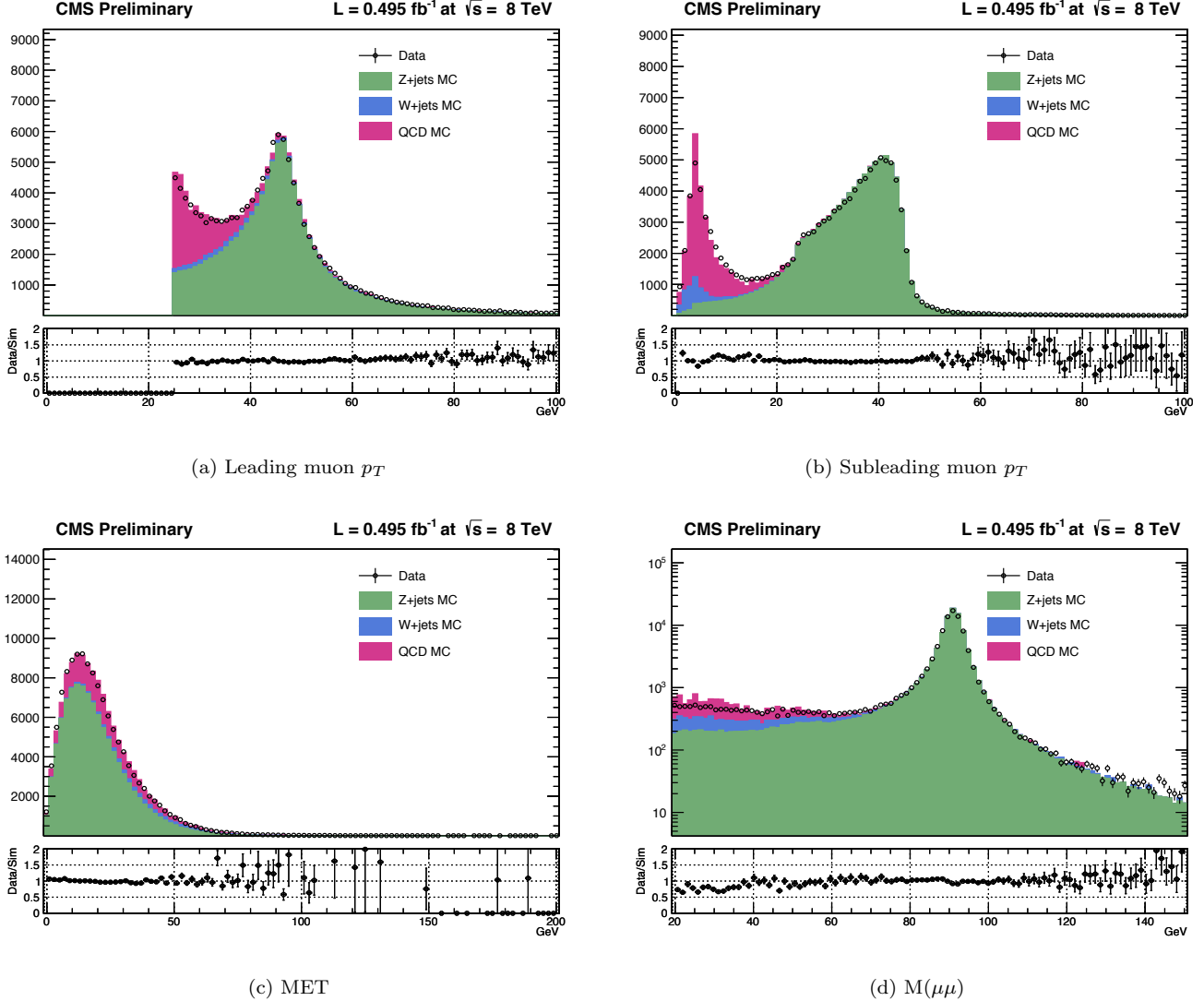


FIG. 3: Data and MC for selection consisting of two muon final states.

is also expected to be genuine missing E_T due to a hard neutrino coming from the W decay. As mentioned in Section III C, a very small pointing angle can also be expected. The following kinematic cuts are used to take advantage of this event topology:

- Leading muon $p_T > 15$ GeV
- MET > 30 GeV
- Sum of distances between individual muons and τ candidate, $\sum \Delta R_{\mu\tau} < .22$

B. Muon ID cuts

As described in Section V, we use two global muons and one track to reconstruct the τ candidate during preselection. We see that a large fraction of QCD background

events passing preselection contain tracks that are actually kaons (K^\pm) or pions (π^\pm) misidentified as muons. Processes containing intermediate heavy mesons can also imitate the vertex topology due to their extremely small lifetime. An example of such a contributing process is

$$\begin{aligned} B^+ &\rightarrow \bar{D}_0 \mu^+ \nu_\mu \\ &\hookrightarrow K^- \pi^+ \\ &\hookrightarrow \mu^- \nu_\mu. \end{aligned}$$

We hence look at muon ID, which tag muons based on a set of selection criteria to each track if it is successfully matched to a reconstructed muon. This is shown in Figure 5. We see that a majority of the lowest- p_T muon tracks are matched to a reconstructed muon for the signal, which is not the case for the background. It is found that requiring all muons to be identified as Particle Flow

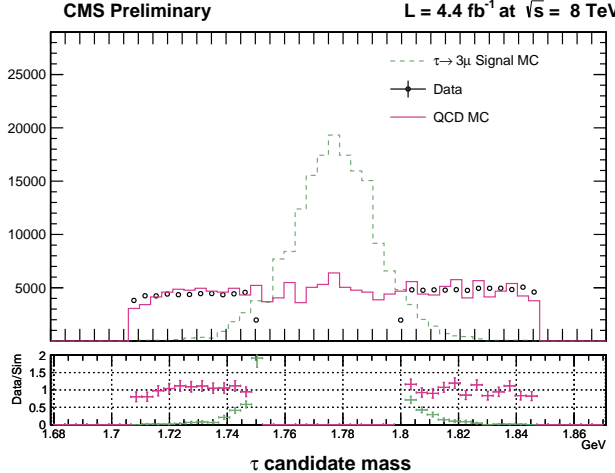


FIG. 4: Three-track invariant mass after preselection showing the signal and control regions.

muons gives the best discriminant against background. See section II B 4 for a brief description of muon identification and reconstruction.

C. Isolation cuts

Muons from $\tau \rightarrow 3\mu$ are relatively isolated, whereas those coming from QCD background are expected to be surrounded by other tracks and jets. Isolation criteria applied to the τ candidate and individual muons provide a powerful discriminant against background. We find isolation information obtained from the Particle Flow algorithm to be especially useful in this case. The following isolation criteria are used, where the sums are over all non-signal particles within the specified cone radius ΔR :

- $\text{RelIso}_{PF}^{\mu_1} \equiv \frac{\sum_{\Delta R < .3} p_T^{\text{PF}}}{p_T^{\mu_1}} < .5$,
- $\text{RelIso}_{PF}^{\mu_2} \equiv \frac{\sum_{\Delta R < .3} p_T^{\text{PF}}}{p_T^{\mu_2}} < .5$,
- $\text{RelIso}_{PF}^{\mu_3} \equiv \frac{\sum_{\Delta R < .3} p_T^{\text{PF}}}{p_T^{\mu_3}} < 1.0$,
- $\text{Iso}_{PF}^{\tau} \equiv \sum_{\Delta R < .4} p_T < 10 \text{ GeV}$
- No more than five tracks within $\Delta R = .4$ of the τ candidate momentum as well as within $\Delta R = .3$ of each muon momentum

Some of these variables are shown in Figure 6.

D. Vertex cuts

The fact that our signal involves the uncommon signature of having three tracks coming from a displaced secondary vertex can be used to exclude background events.

As detailed in Section III C, vertex reconstruction variables are involved in selection at trigger level. Additionally, variables such as the three track SV χ^2 probability and normalized χ^2 are good cut variables and can be further used during selection. We find this is not necessary in our case however, although it may be useful for studies where more statistics are involved or other production modes used.

The vertex reconstruction variables (among others such as pointing angle and tighter isolation criteria) can be used to tighten our selection without making a further significant dent in signal efficiency. Some of the possible cut variables are shown in Figures 6 and 7, and the selection summarized in Table II.

Selection criteria	N_{bkg}	$\epsilon_{\text{sig}} (\%)$
Trigger (HLT_Tau2Mu_1tTrack)	752,439	12.3
Kinematic: $p_T^{\tau} > 15 \text{ GeV}$, $\sum \Delta R_{\mu\tau} < .22$	100,064	8.6
MET $> 30 \text{ GeV}$	28,254	6.1
Muon ID: require PF and tracker)	185	5.1
Isolation: see Section VI C	0	4.8

TABLE II: Event selection criteria. Expected background events are shown for 19.5 fb^{-1} after linearly extrapolating into the signal region.

VII. UPPER LIMITS

Upper limits on cross-section times branching fraction ($\sigma \times \mathcal{B}$) are set using a Bayesian approach with a uniform prior implemented in the macro ROOSTATSCL95^{19,20} recommended by CMS. A large number of pseudo-experiments are performed and the expected limit at 95% CL corresponds to the median value obtained, with the 1σ and 2σ band values determined from the distribution of limits in the pseudo-experiments.

Since our control region had no background after selection, we present the best case scenario of zero background events expected at 19.5 fb^{-1} .

With a signal efficiency of 4.8%, we obtain the upper limit $\sigma(pp \rightarrow WX \rightarrow \tau\nu_{\tau}) \times \mathcal{B}(\tau \rightarrow 3\mu) < 2.9 \times 10^{-3} \text{ pb}$ at 95% CL. Using observed values²¹ for $\sigma(pp \rightarrow WX \rightarrow \tau\nu_{\tau})$ and W branching fractions the PDG²², we obtain $\sigma(pp \rightarrow WX \rightarrow \tau\nu_{\tau}) = 12,910 \text{ pb}$, which gives us the upper limit

$$\mathcal{B}(\tau \rightarrow 3\mu) < 2.3 \times 10^{-7}$$

at 95% CL. This value is roughly an order of magnitude worse than current best experimental upper limits obtained by Belle, BaBar and LHCb.

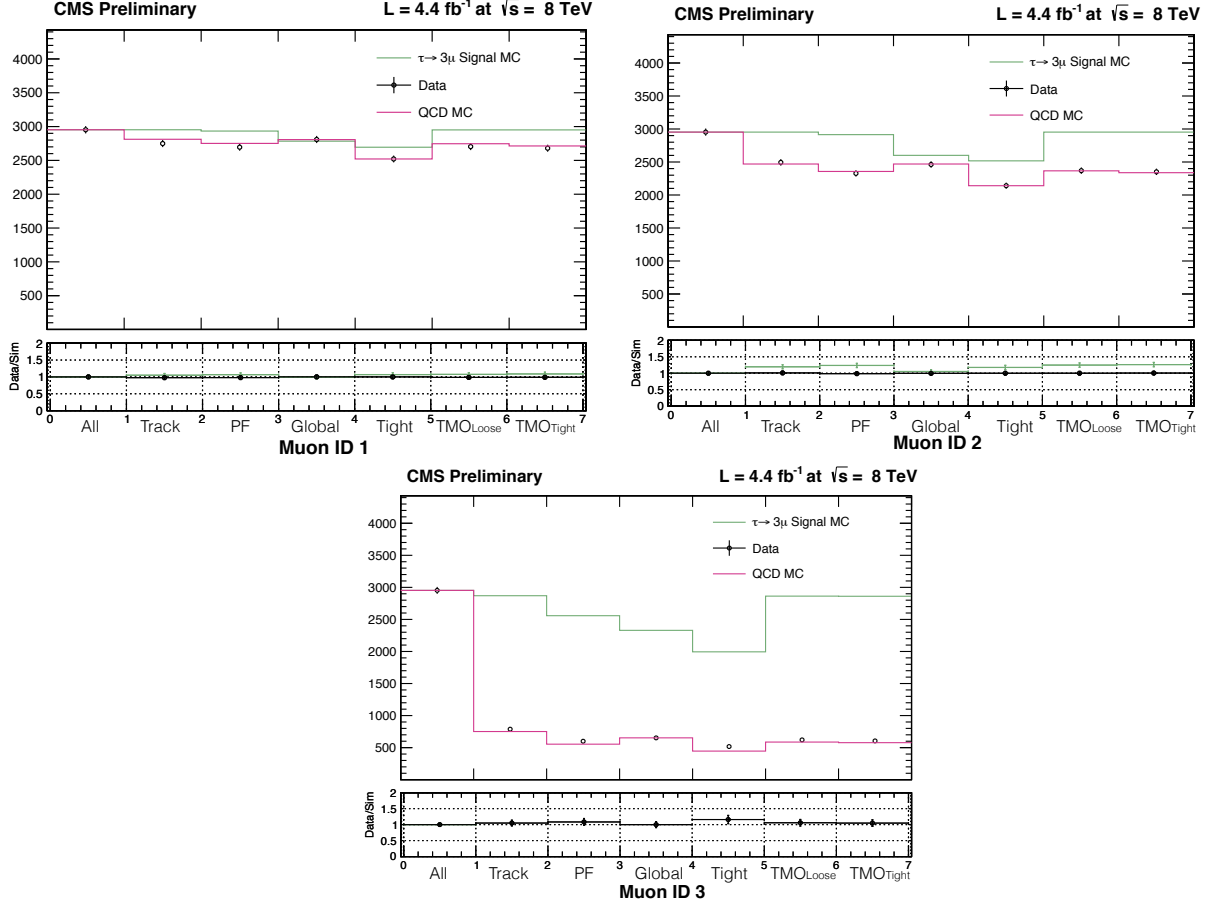


FIG. 5: Muon ID variables associated with the three daughter tracks.

VIII. SUMMARY

We studied the sensitivity of the CMS detector to the lepton flavor violating decay $\tau \rightarrow 3\mu$ using τs from W sources. Signal Monte Carlo was produced and compared with data in the mass sidebands. Sources of background were identified by comparing Monte Carlo samples to data in the sideband control region. A set of cuts were identified in order to improve signal over background discrimination and the control region was finally rendered backgroundless. In this best-case regime, the achievable limit was found to be $\mathcal{B}(\tau \rightarrow 3\mu) < 2.3 \times 10^{-7}$ at 95% CL, which is not competitive with the current best experimental limit of $\mathcal{B}(\tau \rightarrow 3\mu) < 2.1 \times 10^{-8}$ at 90% CL obtained by Belle.

¹M. Raidal et al. Flavor physics of leptons and dipole moments. *The European Physical Journal C*, 57(1-2):13–182, 2008.

²W. J. Marciano et al. Charged Lepton Flavor Violation Experiments. *Ann. Rev. Nucl. Part. Sci.*, 58:315–341, 2008.

³LHCb Collaboration. Measurement of the $B_s^0 \rightarrow \mu^+\mu^-$ branching fraction and search for $B^0 \rightarrow \mu^+\mu^-$ decays at the LHCb experiment. *Phys.Rev.Lett.*, 111:101805, 2013. doi: 10.1103/PhysRevLett.111.101805.

⁴CMS Collaboration. Measurement of the $B_s \rightarrow \mu^+\mu^-$ branching fraction and search for $B_0 \rightarrow \mu^+\mu^-$ with the

CMS Experiment. *Phys.Rev.Lett.*, 111:101804, 2013. doi: 10.1103/PhysRevLett.111.101804.

⁵Belle Collaboration. Search for Lepton Flavor Violating Tau Decays into Three Leptons with 719 Million Produced $\tau^+\tau^-$ Pairs. *Phys.Lett.*, B687:139–143, 2010. doi: 10.1016/j.physletb.2010.03.037.

⁶BaBar Collaboration. Limits on tau Lepton-Flavor Violating decays in three charged leptons. *Phys. Rev. D*, D81:111101, 2010.

⁷LHCb Collaboration. Search for the lepton flavour violating decay $\tau^- \rightarrow \mu^-\mu^+\mu^-$. *LHCb-PAPER-2014-052, CERN-PH-EP-2014-236*, 2014.

⁸Roberto Santinelli and Maurizio Biasini. First Study of the CMS Sensitivity to the Neutrinoless Decay $\tau \rightarrow \mu^+\mu^+\mu^-$. *CERN-CMS-NOTE-2002-037, CMS-NOTE-2002-037*, 2002.

⁹M. Giffels, T. Kress, and A. Stahl. Lepton flavour violation in the neutrinoless tau decay $\tau \rightarrow 3\mu$ with the CMS experiment. *Nucl. Phys. Proc. Suppl.*, 189:317–323, 2009.

¹⁰Lyndon Evans and Philip Bryant. LHC Machine. *JINST*, 3: S08001, 2008.

¹¹CMS Collaboration. CMS physics: Technical design report. *CERN-LHCC-2006-001, CMS-TDR-008-1*, 2006.

¹²CMS Collaboration. The CMS experiment at the CERN LHC. *JINST*, 3:S08004, 2008. doi:10.1088/1748-0221/3/08/S08004.

¹³CMS Collaboration. CMS, the Compact Muon Solenoid. Muon technical design report. *CERN-LHCC-97-32*, 1997.

¹⁴CMS Collaboration. Performance of CMS muon reconstruction in pp collision events at $\sqrt{s} = 7$ TeV. *JINST*, 7:P10002, 2012. doi:10.1088/1748-0221/7/10/P10002.

¹⁵CMS Collaboration. Particle-Flow Event Reconstruction in CMS and Performance for Jets, Taus, and MET. *CMS-PAS-PFT-09-*

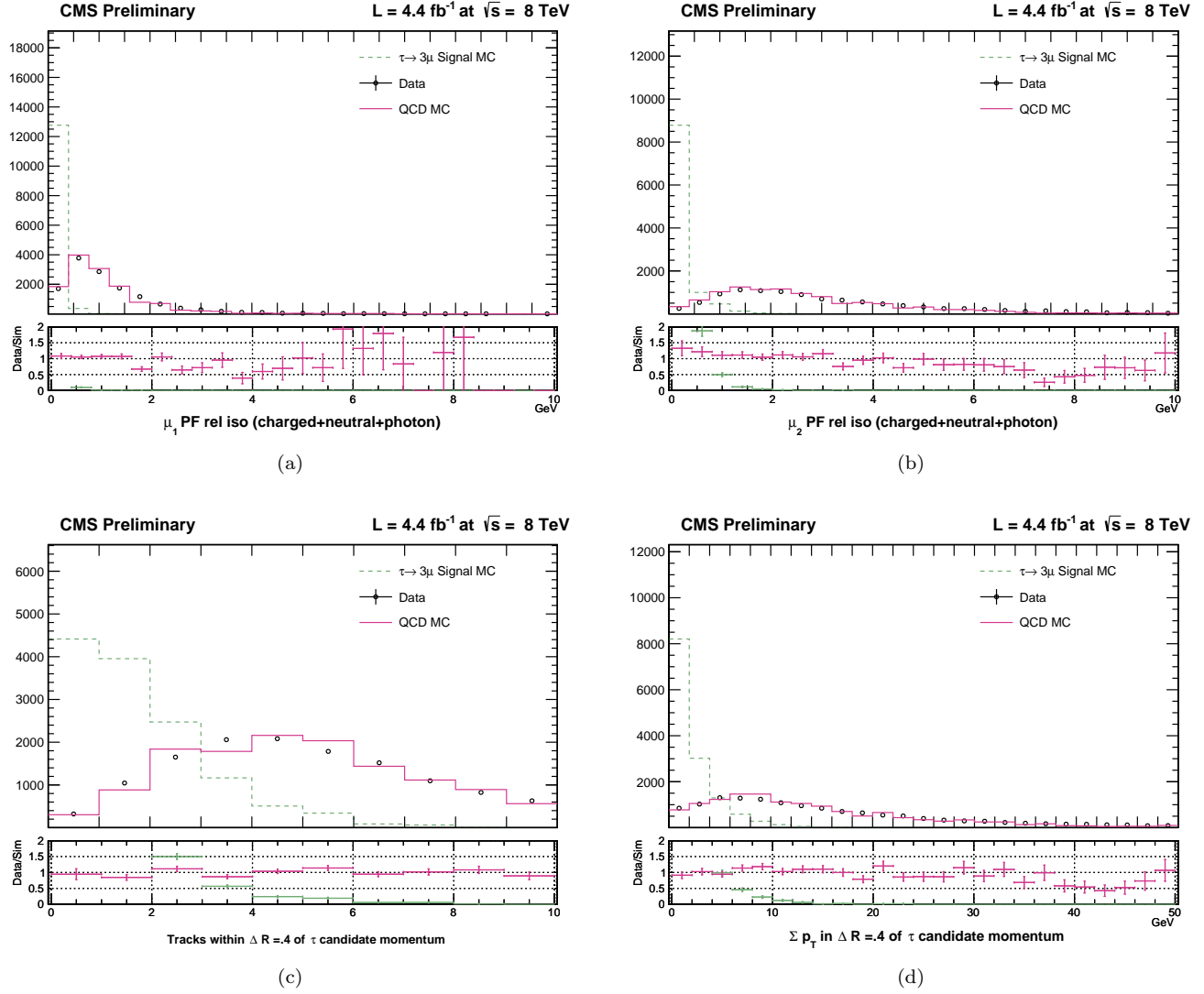


FIG. 6: Sample of isolation variables used in event selection.

- 001, 2009.
¹⁶P. Sphicas. CMS: The TriDAS project. Technical design report, Vol. 2: Data acquisition and high-level trigger. *CERN-LHCC-2002-026*, 2002.
¹⁷R. Frühwirth. Application of Kalman filtering to track and vertex fitting. *Nucl.Instrum.Meth.*, A262:444–450, 1987.
¹⁸G. Punzi. Sensitivity of Searches for New Signals and Its Optimization. In *Statistical Problems in Particle Physics, Astrophysics, and Cosmology*, page 79, 2003.
¹⁹D. Piparo, G. Schott, and G. Quast. RooStatsCms: A tool for analysis modelling, combination and statistical studies. *Journal*

- of Physics Conference Series*, 219(3), 2010.
²⁰L. Moneta, K. Cranmer, G. Schott, and W. Verkerke. The RooStats project. In *Proceedings of the 13th International Workshop on Advanced Computing and Analysis Techniques in Physics Research*, page 57, 2010.
²¹CMS Collaboration. Measurement of inclusive w and z boson production cross sections in pp collisions at $\sqrt{s} = 8$ TeV. *Phys. Rev. Lett.*, 112:191802, 2014.
²²Particle Data Group Collaboration. *Phys. Rev. D*, 86(010001), 2012.

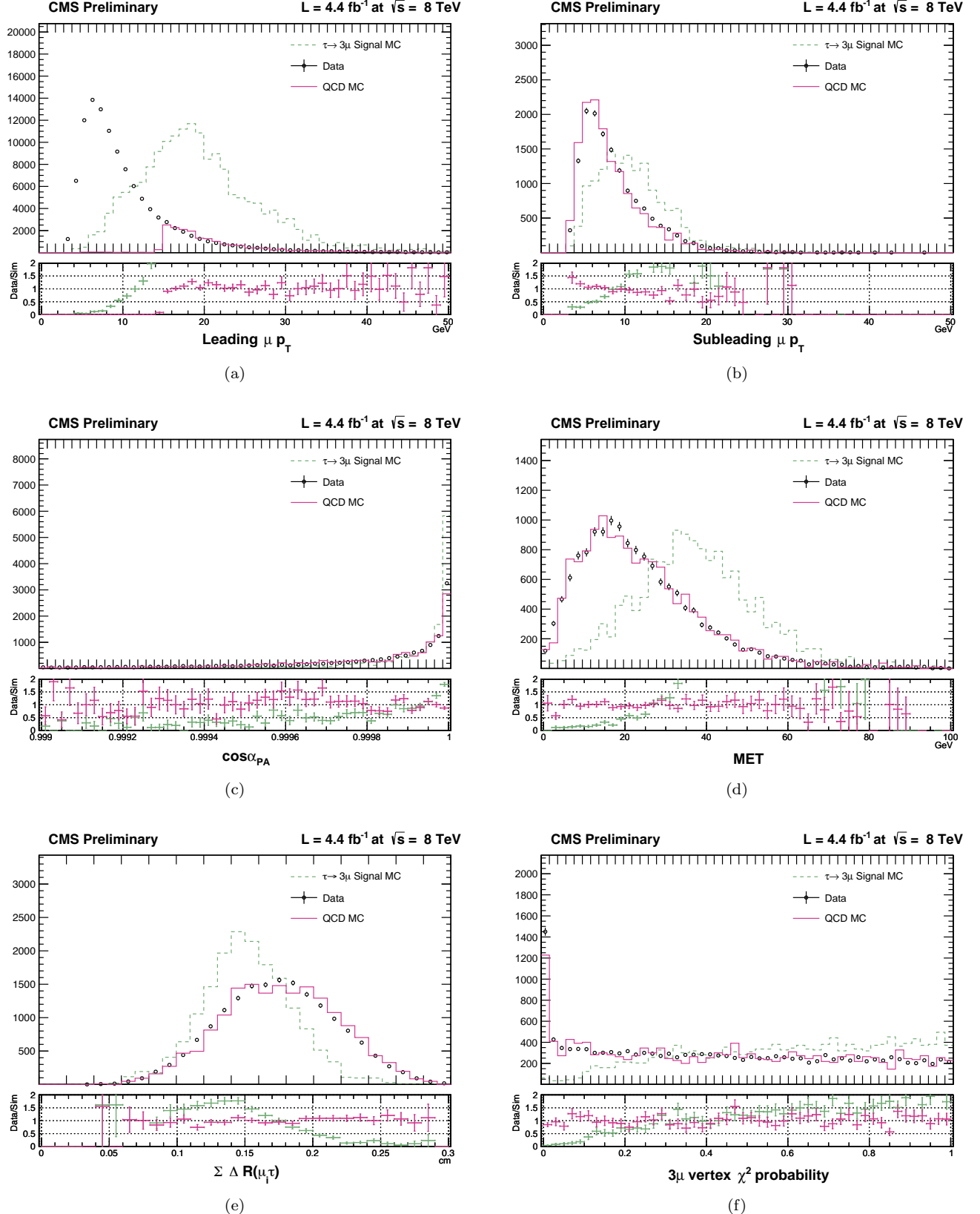


FIG. 7: A selection of variables following preselection. (a) is shown without any further cuts, while the rest are shown after a cut of $p_T^1 > 15$ GeV due to a generator-level cut in the QCD MC.